A Calibration Method for the Higher Modes of a Micro-mechanical Cantilever

N. Shatil,[1, a)] M. E. Homer,[1] L. Picco,[2] P. G. Martin,[2] and O. D. Payton[1, 2]
[1)] *Department of Engineering Mathematics, University of Bristol, BS8 1UB, Bristol, UK*
[2)] *Interface Analysis Centre, University of Bristol, Bristol, BS8 1TL, UK*

(Dated: 12 May 2017)

Micro-mechanical cantilevers are increasingly being used as a characterisation tool in both material and biological sciences. New non-destructive applications are being developed that rely on the information encoded within the cantilever's higher oscillatory modes, such as AFM techniques that measure non-topographic properties of a sample. However, these methods require the spring constants of the cantilever at higher modes to be known in order to quantify their results. Here, we show how to calibrate the micro-mechanical cantilever and find the effective spring constant of any mode. The method is uncomplicated to implement, using only properties of the cantilever and the fundamental mode that are straightforward to measure.

Keywords: MEMS, AFM, Atomic Force Microscope, Cantilevers, Calibration, Higher Modes, Multifrequency, Non-Topography

The use of micro-mechanical sensors (MEMS) has increased dramatically over the last fifteen years, becoming a vital tool in fields such as diagnostics, photothermal spectroscopy, and mass and chemical detection; they are also at the heart of scanning probe microscopy, such as the atomic force microscope (AFM)[1–5]. AFMs have been used extensively to map sample topography to nanometre resolution, and new techniques are extending their operating potential beyond topography to include measurements of properties such as the hardness, viscoelasticity and stiffness of a sample[6,7]. These non-topographic techniques have already been applied within material and biological sciences to both hard and soft samples; the ability to find non-topographic properties is of particular importance when seeking to minimise damage[8].

Non-destructive techniques often use micro-cantilevers with low spring constants to avoid potential damage, by exciting the cantilever until the effective stiffness at a resonant frequency matches that of the sample or the surrounding medium[9,10]. Then, the combination of the shift in resonant frequency at a specific mode and a suitable model of the cantilever-sample interaction leads to measurements of the investigated property. However, methods that utilise the higher modes have been restricted to relative results[11,12]; their quantification requires the ability to determine with confidence the effective spring constant of a cantilever oscillating free from a sample at arbitrary mode number. In this paper, we describe a method that resolves this problem in a way that is both repeatable and straight-forward.

Many calibration methods exist for finding the spring constant at the first or fundamental mode[13]. They typically seek to avoid using properties of a cantilever that are difficult to measure, such as thickness or density. For example, conventional AFM probes have a total thickness of less than a micron and include a gold layer, to boost reflectiveness, that has a thickness of some tens of nanometres. The composite structure and small thicknesses are challenging to quantify accurately, and so many existing techniques instead use indirect means of calibration. For example, the Sader method[14] uses fluid dynamics to estimate the hydrodynamic effect on a cantilever's resonant frequencies, and does not require knowledge of the thickness, density or Young's modulus of the cantilever. Alternatively, the thermal method[15] uses the equipartition theorem to relate the power spectrum of a thermally excited cantilever to its resonant energy in order to find the spring constant, also avoiding reliance on difficult to measure properties.

While these methods can be applied to determine the stiffness of higher modes of the cantilever, they face limitations as the mode number increases. The reliance on thermal excitations means that the thermal method restricts calibration in practice to only the first few modes for many micro-mechanical cantilevers. The Sader method depends on the accuracy of theories that describe flow around a cantilever, which are difficult to verify experimentally at high mode number. Issues include the assumption that the Reynolds number of the flow is small, and that the method (in its simplest form) considers only two-dimensional flow across the cantilever width[14]. However, at high mode number both the Reynolds number increases and flow along the length of the cantilever has been shown to dominate[16]. While extensions to the fluid theory have been proposed to address these limitations[17,18], we instead show how the material properties of the cantilever can be found and used to circumvent such difficulties.

By focussing on the material properties of the cantilever, our method is not limited by mode number, and can be used as a check against other calibration techniques without the need for additional analysis or measurements. It uses only the (experimentally measurable) Q-factor and resonant frequency at the first mode, without the need for additional parameter fitting. The method is summarised by the following steps:

[a)] Electronic mail: Nam.Shatil@bristol.ac.uk

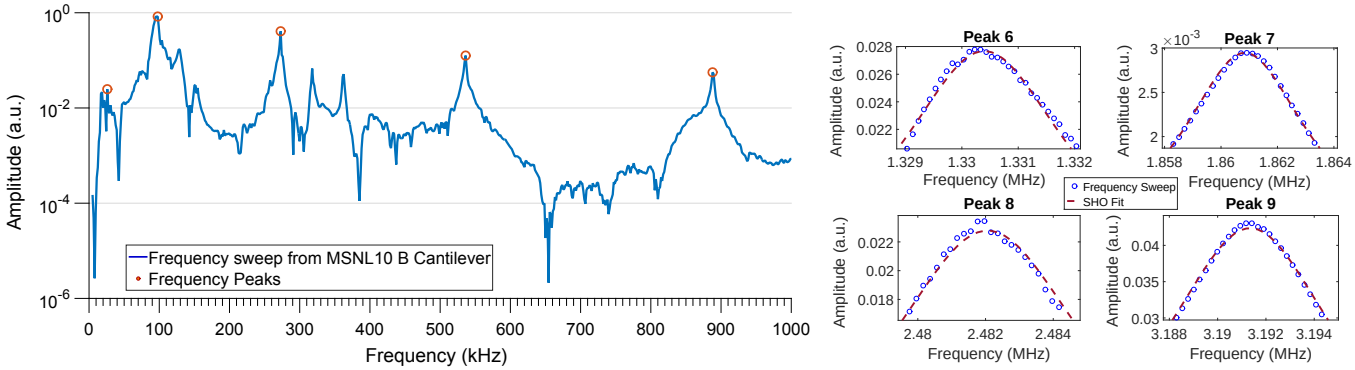

(a) (b)

FIG. 1: (a) A sample frequency response obtained by driving a rectangular MSNL-10B Bruker cantilever with a lock-in amplifier, where amplitude is displayed in log scale, with arbitrary units (a.u.) and normalised to the amplitude of the second mode. The apparent low amplitude of the fundamental mode is due to the use of a 15kHz high pass filter to improve the signal to noise ratio in higher modes. The amplitude of the fundamental mode was measured separately without this filter in place. This corresponds to frequency sweep V. (b) Detail of the frequency response (circles, blue) and simple harmonic oscillator curve fits for modes six to nine (dashed line, red).

- The spring constant depends on the flexural rigidity, the length of the cantilever and the wave number of the specified mode.
- The flexural rigidity in turn depends on the structure of the cantilever. In a rectangular AFM cantilever, this is determined by the length, breadth, and two unknown thicknesses — the total thickness of the cantilever and the thickness of the gold layer — together with the densities of the two layers.
- To find the unknown thicknesses, we solve two simultaneous equations that link the material properties of the cantilever to the resonant frequency and Q-factor of the first mode. The first equation is a combination of the flexural rigidity of a composite beam with the equation for its resonant frequency in vacuo and the shift in resonance due to the surrounding fluid, obtained from standard cantilever models, while the second is the rule of mixtures for composite materials.
- The effective stiffness is then found by combining the length and flexural rigidity of the cantilever with the wave number of the specified mode.

We demonstrate our method for the case of a rectangular AFM cantilevered probe oscillating in air (though it is applicable to any cantilever-based sensor), and compare our results against other calibration methods. The effective spring constant of the n^{th} mode of a rectangular cantilever is given by the fundamental relation,[19]

$$k_n = 0.2427 \mu L \omega_{n,\text{vac}}^2, \tag{1}$$

where μ is the mass per unit length, L is the length and $\omega_{n,\text{vac}}$ is the resonant frequency of the n^{th} mode (in vacuo) of the cantilever. The aim of our approach is to use information measured at the first mode to calculate μ and then use an analytic model of the cantilever as a composite beam to find $\omega_{n,\text{vac}}$. The effective spring constant is then given by applying Eq. (1) at any desired mode. The measured shift in resonant frequency from $\omega_{n,\text{vac}}$ can be used to measure the additional effect on the cantilever due to the surrounding fluid, as described below.

The mass per unit length, $\mu = \rho_c h_T b$, is the product of the total thickness, h_T, width, b, and density, ρ_c, of the cantilever. To avoid the need to measure these properties, we instead use the relation[14]

$$\mu = \frac{\pi b^2 \rho_f}{4} \left(Q_{1,R} \Gamma_i(\omega_{1,R}) + \Gamma_r(\omega_{1,R}) \right), \tag{2}$$

at the first mode, where $Q_{1,R}$ and $\omega_{1,R}$ are the measured Q-factor and resonant frequency at the first mode, ρ_f is the density of the surrounding fluid, Γ is the hydrodynamic loading function[14] and subscripts r and i denote the real and imaginary parts respectively. This is based on the Sader method which has been shown to find the effective spring constant at the first mode to within 5% accuracy[20], giving us confidence in Eq. (2).

To find $\omega_{n,\text{vac}}$, we choose for simplicity to model the cantilever as an Euler-Bernoulli beam; the deflection $w(x,t)$ is given by

$$\frac{\partial^4 w(x,t)}{\partial x^4} + \frac{\mu}{EI} \frac{\partial^2 w(x,t)}{\partial t^2} = F, \tag{3}$$

for a beam with flexural rigidity EI, driven by a force F, with boundary conditions $w = w_x = 0$ at $x = 0$ and $w_{xx} = w_{xxx} = 0$ at $x = L$. Solving gives the resonant frequency of the cantilever in vacuo

$$\omega_{n,vac} = \left(\frac{\alpha_n}{L} \right)^2 \sqrt{\frac{EI}{\mu}}, \tag{4}$$

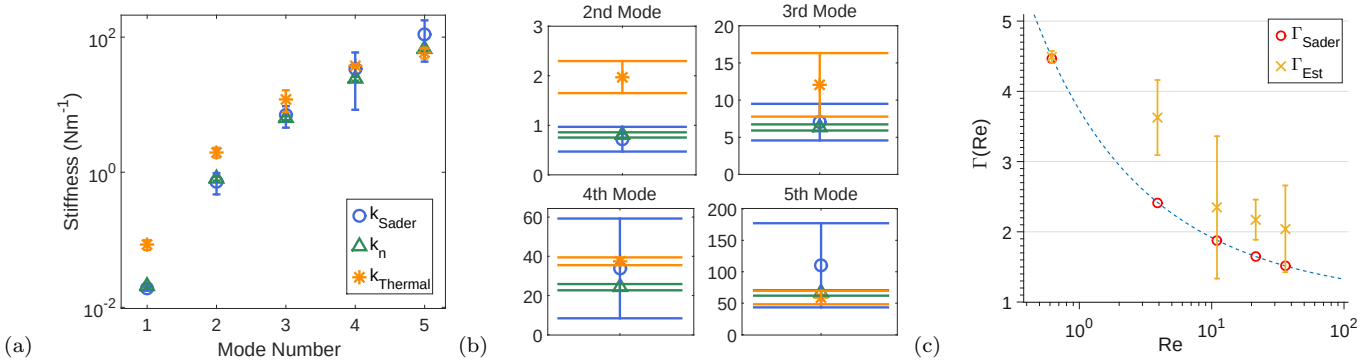

FIG. 2: (a) The effective spring constant found our method, the Sader method, and the thermal method. (b) A zoom in on the effective stiffness and variation for modes 2-5 found using each method. (c) The additional loading due to the surrounding fluid, $\Gamma_{\rm Est}$ estimated by Eq. (6), compared to the Sader method[14]. The dotted line is the real part of the hydrodynamic function, $\Gamma(\omega)$ and circles are the Reynolds number for each mode.

where α_n is the eigenvalue of the $n^{\rm th}$ mode. The analytic model, Eq. (3), can be adjusted to include other considerations such as tip mass, tip positioning, irregular cantilever geometries (e.g., V-shaped), and height changes[21,22]. One way to verify the model is to compare the mode shapes given by calculation of α_n and characteristic equation, to measurements of the deflection of the cantilever taken incrementally across the length using a laser doppler vibrometer[23] (see Supplementary Fig. S1, which shows good agreement for our chosen AFM probe). Note, though, that the method is applicable without such equipment or comparison.

Substituting Eq. (4) into Eq. (1) gives the effective spring constant, assuming that EI is known. While this is straightforward for a uniform cantilever, typical AFM cantilevers also include a thin gold layer. Despite being neglected in many calibration techniques, it does have significantly different material properties to typical MEMS materials such as silicon and silicon nitride, and can have a sizeable effect as we show below. We assume that the cantilever is a two-layer composite, with a gold layer of thickness, $h_{\rm Au}$, and density, $\rho_{\rm Au}$, added to the cantilever body, $h_{\rm T}$, with density, $\rho_{\rm Si}$. Laminar beam theory[24] gives the flexural rigidity of the composite cantilever as

$$EI = \frac{b}{24}\left[E_{\rm Si}\left(h_{\rm T}^3 + H^3\right) + E_{\rm Au}\left(h_{\rm T}^3 - H^3\right)\right] \qquad (5)$$

where $H = h_{\rm T} - 2h_{Au}$. In order to find $h_{\rm T}$ and h_{Au}, we use the shift in resonant frequency of the first mode due to the presence of the surrounding medium[14]

$$\omega_{1,vac} = \omega_{1,\rm R}\left(1 + \left(\frac{\pi b^2 \rho_{\rm f}}{4\mu}\right)\Gamma_{\rm r}(\omega_{1,\rm R})\right)^{\frac{1}{2}} = \left(\frac{\alpha_1}{L}\right)^2\sqrt{\frac{EI}{\mu}}. \qquad (6)$$

Substituting Eq. (5) into Eq. (6 gives one equation for $h_{\rm Au}$ and $h_{\rm T}$; this, together with the rule of mixtures for composite materials[25]

$$b\left(h_{\rm Au}(\rho_{\rm Au} - \rho_{\rm Si}) + h_{\rm T}\rho_{\rm Si}\right) = \mu \qquad (7)$$

gives two simultaneous equations for the two unknown thicknesses, h_{Au} and $h_{\rm T}$, in terms of readily measurable quantities (resonant frequency and Q-factor of the first mode, $\omega_{1,\rm R}$, $Q_{1,\rm R}$, length and breadth of the cantilever, L, b, and the mass per unit length, Eq. (2)):,

$$\begin{aligned} b\left(h_{\rm Au}(\rho_{\rm Au} - \rho_{\rm Si}) + h_{\rm T}\rho_{\rm Si}\right) &= \mu, \\ \frac{b}{24}\left[E_{\rm Si}\left(h_{\rm T}^3 + H^3\right) + E_{\rm Au}\left(h_{\rm T}^3 - H^3\right)\right] &= \\ \mu\left(\frac{L}{\alpha_1}\right)^4\omega_{1,\rm R}^2\left(1 + \left(\frac{\pi\rho_{\rm f}b^2}{4\mu}\right)\Gamma_r(\omega_{1,\rm R})\right). & \end{aligned} \qquad (8)$$

These equations can be solved numerically, and the results inserted into Eqs. (5), (4) and (1) to give the effective stiffness.

To demonstrate our technique, we have taken measurements of the spectra of five different MSNL-10B Bruker rectangular cantilevers, driven by both thermal excitations (using a custom-built AFM at the University of Bristol[26]), and also a piezo-electric actuator and a lock-in amplifier (Zurich Instruments HS2Li); see Figs. 1a, and S5- S7. Simple harmonic oscillator (SHO) equations were fitted to each resonant peak (Fig. 1b), and the effective spring constants found from Eq. (1), using the method described above. The results are shown in Fig. 2a, together with those obtained from the Sader and thermal methods, for comparison.

When calculating the effective spring constant, our method gave consistent values across repeated measurements; see Table II and Fig. 2a. However, we saw less variation in the values obtained from our method than either the Sader method or thermal method. By driving the cantilever directly with piezo-electric actuators and the lock-in amplifier, we were able to excite the cantilever up to 2 MHz, which corresponds to the cantilever's tenth bending mode. Again we observed good agreement between the effective stiffnesses predicted by our method and those of the Sader method; see Supplementary Table SIV. However, the variation between experiments (using the same cantilever) increases significantly with mode

number for the Sader method (see Fig. 2a and Table II), and requires the additional fitting of SHO equations for each mode. In contrast, our method is able to find the effective stiffness with consistently low variation, using only the measured resonant frequency and Q factor at the first mode. Therefore, we believe that it is robust at finding the effective spring constant of higher modes.

In addition, we can reliably calculate material properties of the cantilever. Table I shows our predictions of cantilever thickness, h_{T}, gold layer thickness h_{Au}, spring constant, k_1 and those given by the manufacturer. The gold layer is given as (45 ± 5) nm and the total thickness as (0.55 ± 0.05) µm. Across the five frequency sweeps, we find the mean total thickness to be 0.537 µm with a standard deviation of 0.018 nm, and the mean thickness of the gold layer to be 30.6 nm with a standard deviation of 9.65 nm. The SEM images showed the total thickness to be approximately 0.6 µm, but it was difficult to discern the thickness of the gold layer due to the charging effects on the insulating silicon. However, when the gold layer was ignored from our calculations we found that the frequency of resonance in vacuo, ω^*_{vac}, was estimated higher than the measured resonance by as much as 35%, emphasising that the gold layer has a significant effect.

Eq. (6) can be used to calculate the additional loading on the cantilever from the surrounding air; we found it to overestimate the fluid loading predicted by the hydrodynamic function[14] with a large spread of potential values, predominantly due to small changes in the measured resonant frequency; see Fig. 2c. However, the actual shift in measured resonant frequency from the calculated resonant frequency in vacuo was less than 2% at the first mode and less than 1% from the fifth mode onwards. This corresponds to a less than 5% difference in the effective spring constant. Taken together, these give confidence that our method does indeed accurately predict the effective spring constants of any mode of a micro-mechanical cantilever.

See supplementary material for information about the experimental measurements of the MSNL-10B Bruker cantilevers. It includes the deflection of the thermally excited cantilever as measured with the LDV and compared to the analytic mode shapes, (Fig. S1), the SEM images of the cantilever, (Supplementary Figures S2, S3 and S4), and the additional power spectrum of the cantilevers (Supplementary Figures S5, S6 and S7). We also include the tabulated results comparing our method to the Sader method and the thermal method (Supplementary Tables SI, SII, SIII and SIV).

The authors gratefully acknowledge the Low Noise Labs of the NSQI Centre at the University of Bristol for hosting the custom AFM. Shatil was supported by a UK Engineering and Physical Sciences Research Council (EPSRC) CASE award, in collaboration with Sellafield Ltd. and EDF Energy, Nuclear Generation Ltd. Payton was supported by the Royal Academy of Engineering.

TABLE I: The thicknesses, h_{T} and h_{Au}, Q-factor, Q, measured resonant frequency, $\omega_{1,\mathrm{R}}$, and estimated resonant frequency, $\omega^*_{1,\mathrm{vac}}$, found using Eq. (4) and ignoring the influence of the additional gold layer, as well as the effective spring constant of the first mode, k_1, found using our method for frequency sweeps I.-V.

	$h_{\mathbf{T}}$ (µm)	h_{Au} (nm)	Q -	$\omega_{1,\mathbf{R}}$ (kHz)	$\omega^*_{1,\mathbf{vac}}$ (kHz)	k_1 (Nm^{-1})
Manufacturers	0.55	45	-	15	-	0.0200
I. (Thermal)	0.547	37	21	15.1	20.7	0.0212
II. (Thermal)	0.524	29	19	14.7	18.1	0.0194
III. (Thermal)	0.553	36	21	15.1	18.2	0.0215
IV. (Lock-In)	0.549	36	21	14.9	18.1	0.0217
V. (Lock-In)	0.509	14	17	15.5	18.1	0.0187

TABLE II: Predicted effective spring constant (mean, standard deviation) of modes 1–5, found using our method, (k_n, σ_n), the Sader method, $(k_{\mathrm{Sader}}, \sigma_{\mathrm{Sader}})$, and the thermal method, $(k_{\mathrm{Thermal}}, \sigma_{\mathrm{Thermal}})$. All units are Nm^{-1}.

Mode	k_n	σ_n	$k_{\mathbf{Sader}}$	$\sigma_{\mathbf{Sader}}$	$k_{\mathbf{Thermal}}$	$\sigma_{\mathbf{Thermal}}$
1	0.0205	0.0013	0.019	0.0014	0.0846	0.014
2	0.806	0.0527	0.719	0.249	1.97	0.324
3	6.32	0.413	7.03	2.46	12.0	4.27
4	24.3	1.59	33.8	25.4	37.4	1.98
5	66.3	4.33	110	66.9	59.0	10.8

[1] K. L. Ekinci, Y. T. Yang, and M. L. Roukes, J. Appl. Phys. **95**, 2682 (2004).
[2] J. R. Barnes, R. J. Stephenson, M. E. Welland, C. Gerber, and J. K. Gimzewski, Nature **372**, 79 (1994).
[3] J. Fritz, M. K. Baller, H. P. Lang, H. Rothuizen, P. Vettiger, E. Meyer, H. Güntherodt, C. Gerber, and J. K. Gimzewski, Science **288**, 316 (2000).
[4] H. P. Lang, R. Berger, F. Battiston, J. P. Ramseyer, E. Meyer, C. Andreoli, J. Brugger, P. Vettiger, M. Despont, T. Mezzacasa, L. Scandella, H. J. Güntherodt, C. Gerber, and J. K. Gimzewski, Appl. Phys. A - Mater. **66**, 61 (1998).
[5] G. Binnig, C. Gerber, and C. Quate, Macromolecules **56** (1986).
[6] S. Kawai, T. Glatzel, S. Koch, B. Such, A. Baratoff, and E. Meyer, Phys. Rev. Lett. **103**, 220801 (2009).
[7] D. Forchheimer, S. S. Borysov, D. Platz, and D. B. Haviland, Nanotechnology **25**, 485708 (2014).
[8] H. Dankowicz, Phil. Trans. Roy. Soc. A **364**, 3505 (2006).
[9] R. J. Clarke, V. Bachtiar, T. C. Lee, J. E. Cater, and J. Minton, J. Appl. Phys **117** (2015).
[10] D. C. Hurley, S. E. Campbell, J. P. Killgore, L. M. Cox, and Y. Ding, Macromolecules **46**, 9396 (2013).
[11] C. Held, T. Seyller, and R. Bennewitz, Beilstein J. of Nanotechnology **3**, 179 (2012).
[12] J. R. Lozano and R. Garcia, Phys. Rev. Lett. **100**, 076102 (2008).
[13] J. te Riet, A. J. Katan, C. Rankl, S. W. Stahl, A. M. van Buul, I. Y. Phang, A. Gomez-Casado, P. Schön, J. W. Gerritsen, A. Cambi, A. E. Rowan, G. J. Vancso, P. Jonkheijm, J. Huskens, T. H. Oosterkamp, H. Gaub, P. Hinterdorfer, C. G. Figdor, and S. Speller, Ultramicroscopy **111**, 1659 (2011).
[14] J. E. Sader, J. Appl. Phys. **84**, 64 (1998).
[15] H. J. Butt and M. Jaschke, Nanotechnology **6**, 1 (1995).

[16] A. Maali, C. Hurth, R. Boisgard, C. Jai, T. Cohen-Bouhacina, and J. P. Aime, J. Appl. Phys. **97**, 074907 (2005).
[17] C. A. Van Eysden and J. E. Sader, J. Appl. Phys. **101**, 044908 (2007).
[18] A. Tafuni and I. Sahin, J. Fluid. Struct. **52**, 101 (2015).
[19] J. E. Sader, J. W. M. Chon, and P. Mulvaney, Rev. Sci. Instrum. **70**, 3967 (1999).
[20] N. A. Burnham, X. Chen, C. S. Hodges, G. A. Matei, E. J. Thoreson, C. J. Roberts, M. C. Davies, and S. J. B. Tendler, Nanotechnology **14**, 1 (2003).
[21] Y. M. Tseytlin, Rev. Sci. Instrum. **79**, 059901 (2008).
[22] M. S. Allen, H. Sumali, and P. C. Penegor, J. Dyn. Syst. Meas. Control **131**, 064501 (2009).
[23] O. D. Payton, L. Picco, A. R. Champneys, M. E. Homer, M. J. Miles, and A. Raman, Rev. Sci. Instrum. **82**, 043704 (2011).
[24] J. R. Vinson and R. L. Sierakowski, Springer Netherlands **5** (1987).
[25] B. Harris, *Engineering Composite Materials* (Institute of Metals, London, 1986).
[26] O. D. Payton, L. Picco, and T. B. Scott, Int. Mater. Rev. **61**, 473 (2016).

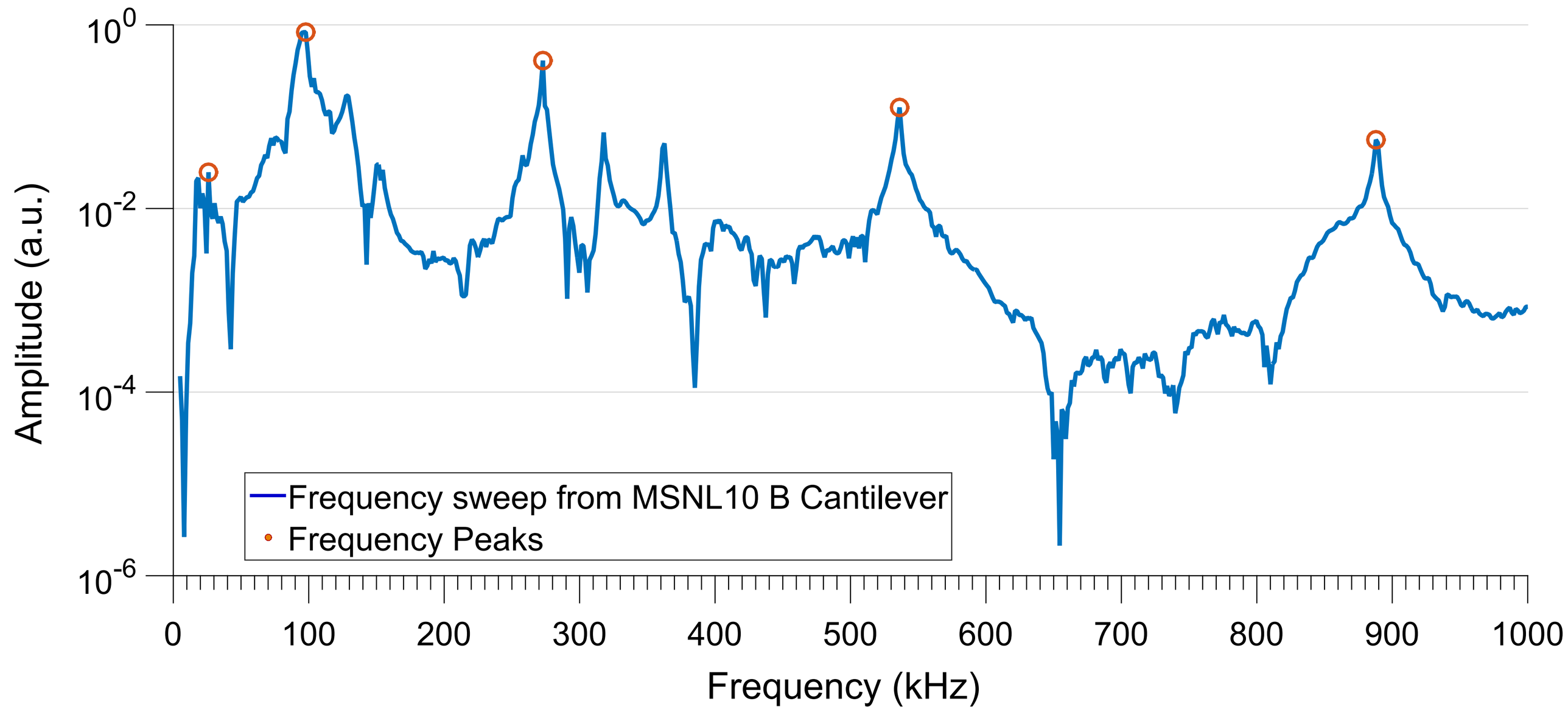
Amplitude (a.u.)
10^{0}
10^{-2}
10^{-4}
10^{-6}
0
100
200
300
400
500
600
700
800
900
1000
Frequency (kHz)
Frequency sweep from MSNL10 B Cantilever
Frequency Peaks

Peak 6

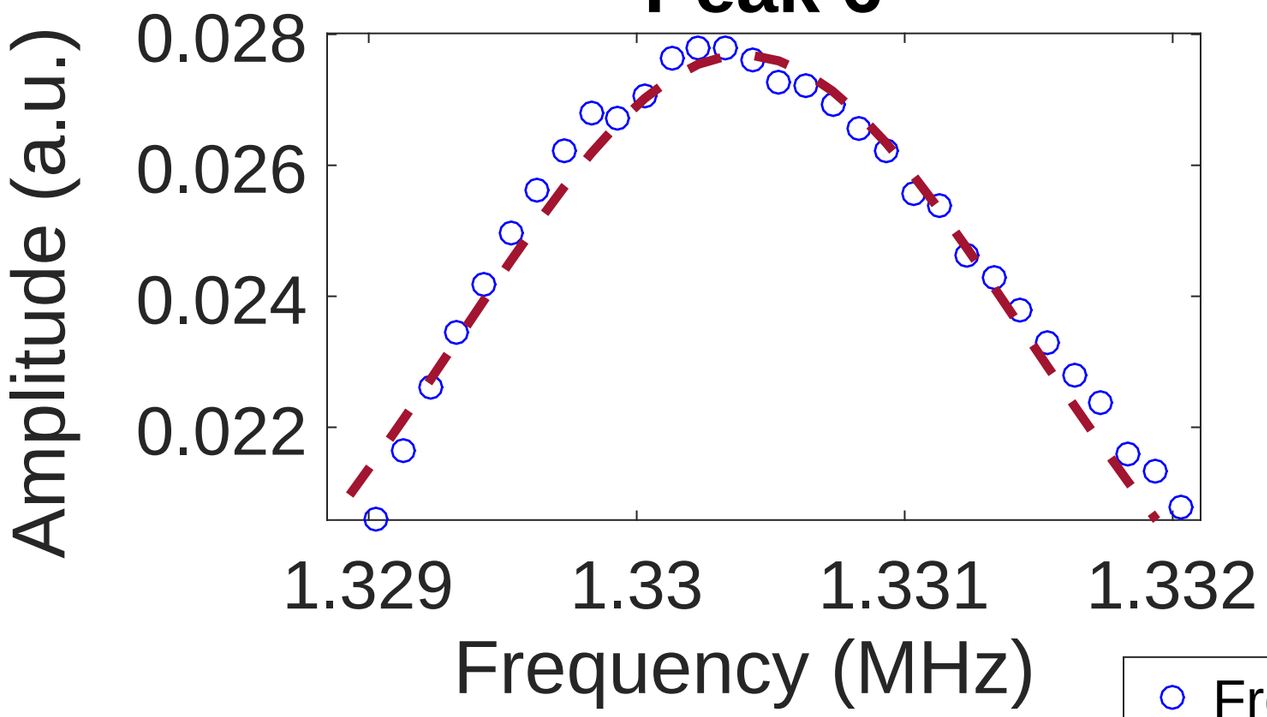

Peak 7

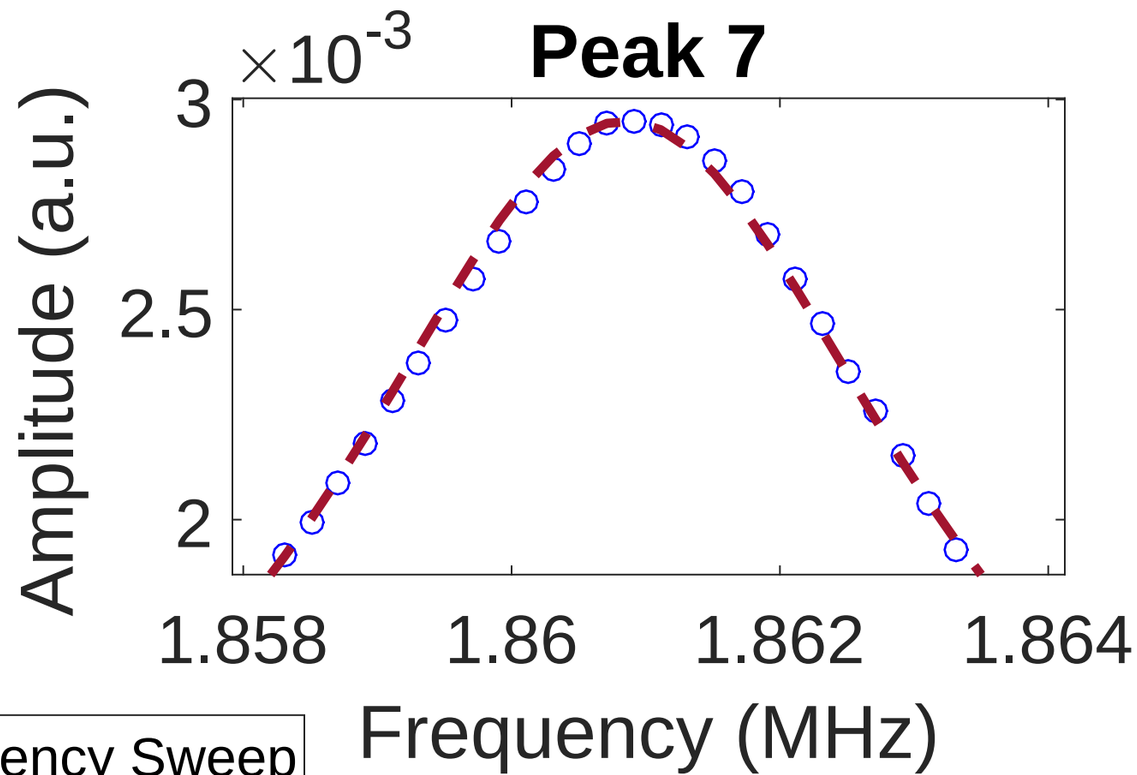

Peak 8

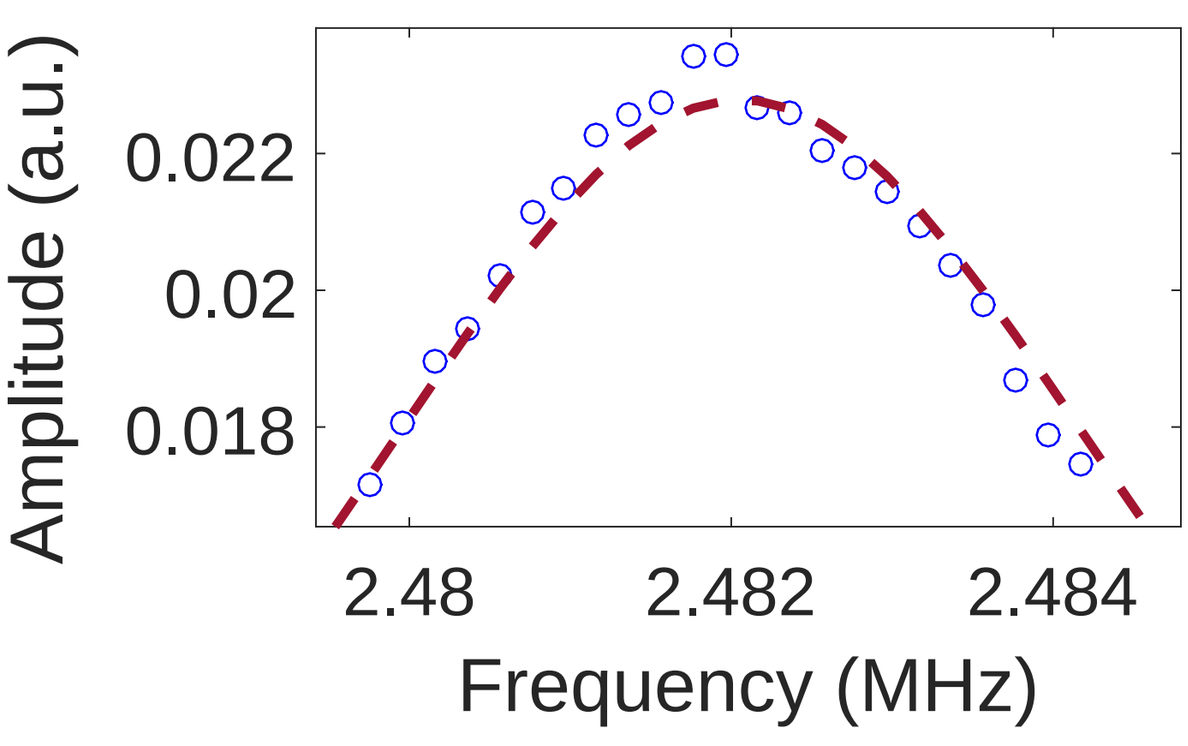

Peak 9

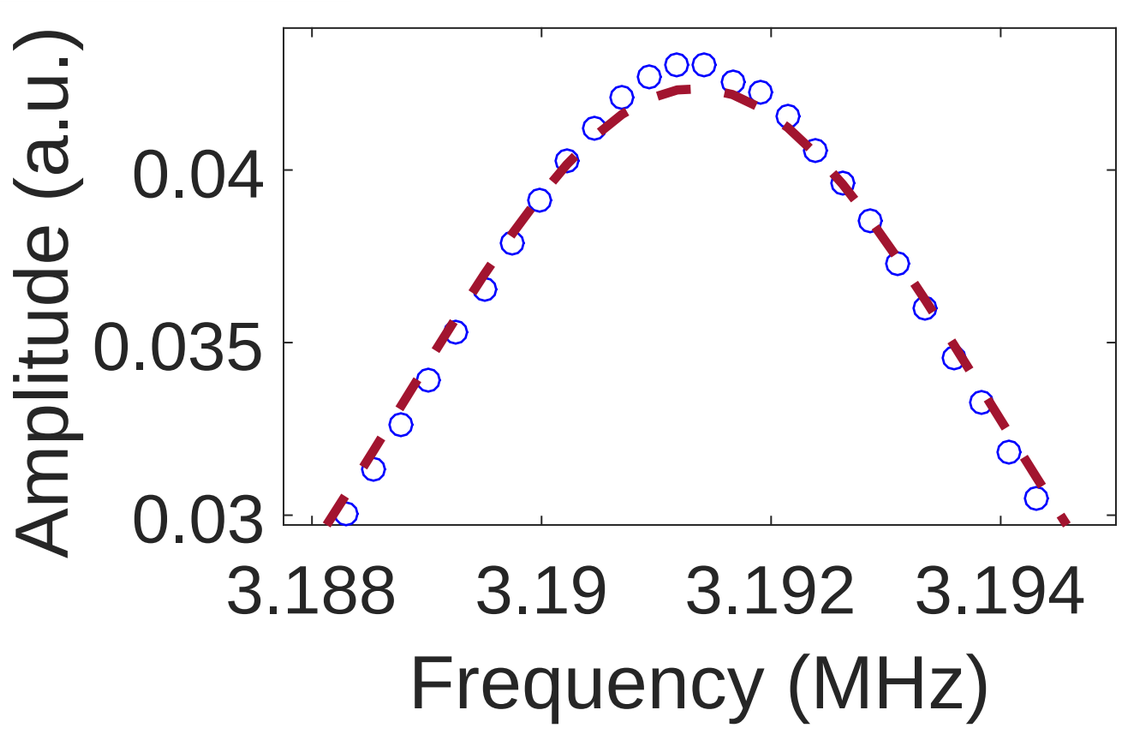

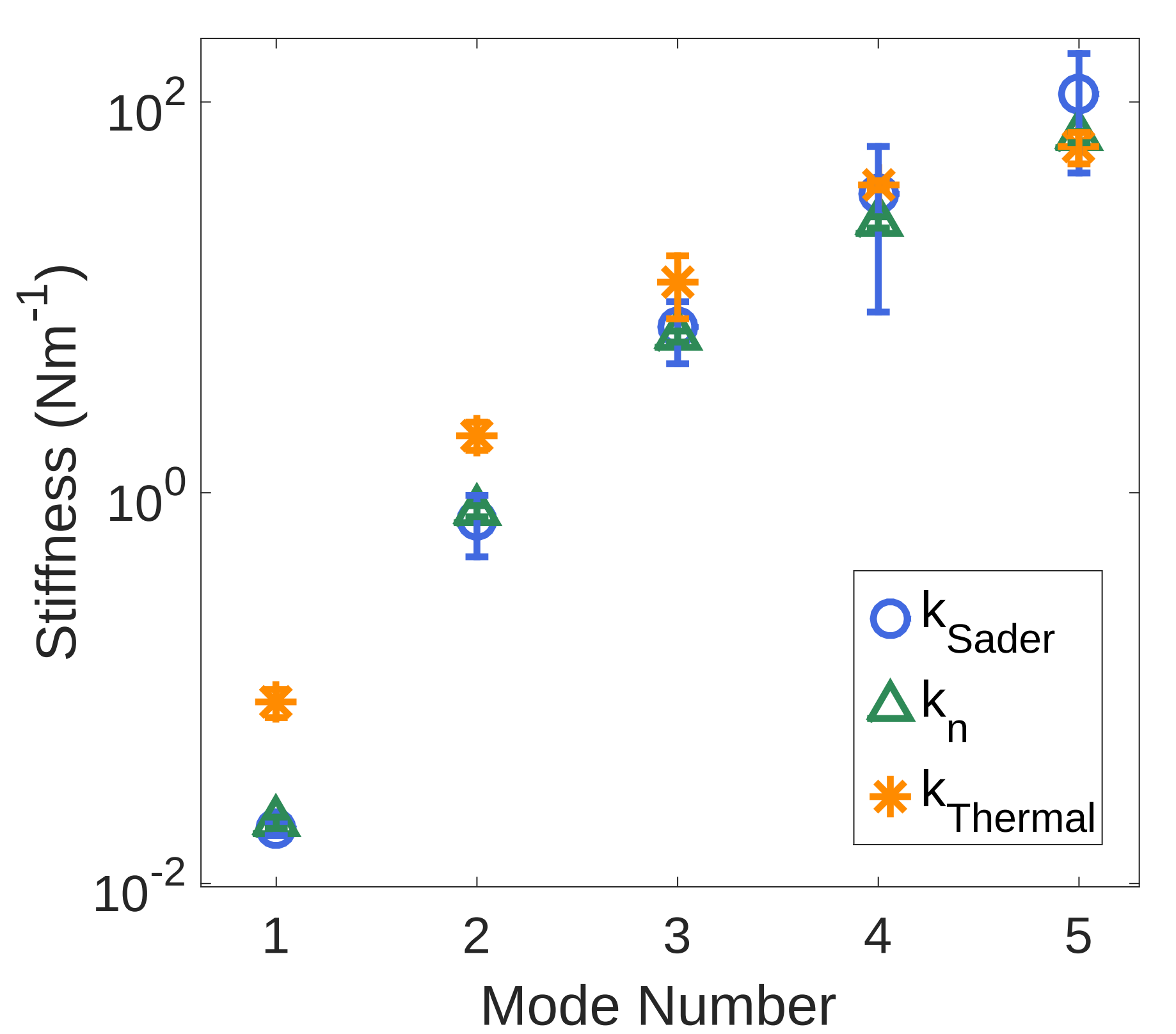
10^2
10^0
10^{-2}
Stiffness (Nm^{-1})
1
2
3
4
5
Mode Number
k_{Sader}
k_n
$k_{Thermal}$

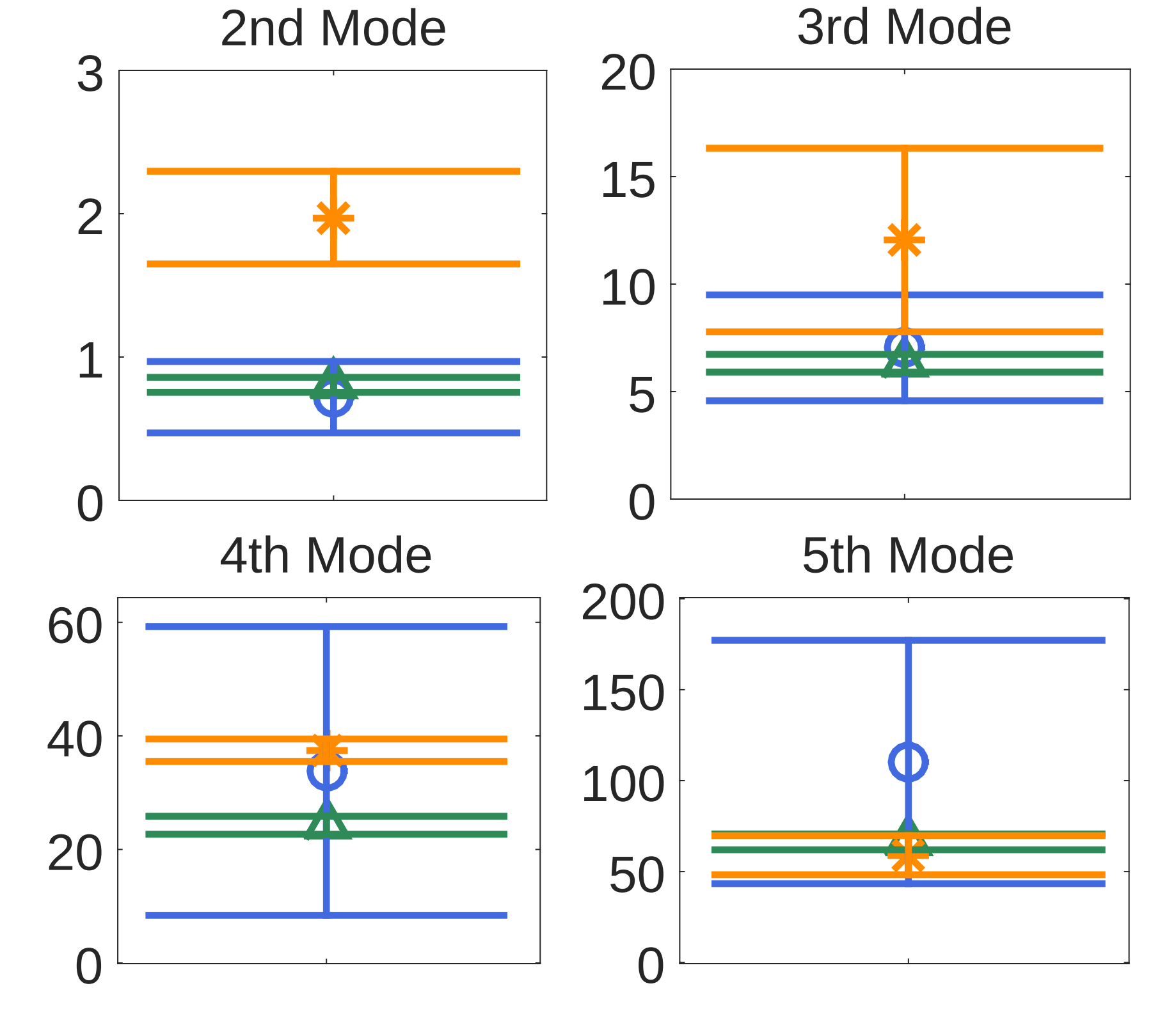
2nd Mode
3
2
1
0
3rd Mode
20
15
10
5
0
4th Mode
60
40
20
0
5th Mode
200
150
100
50
0

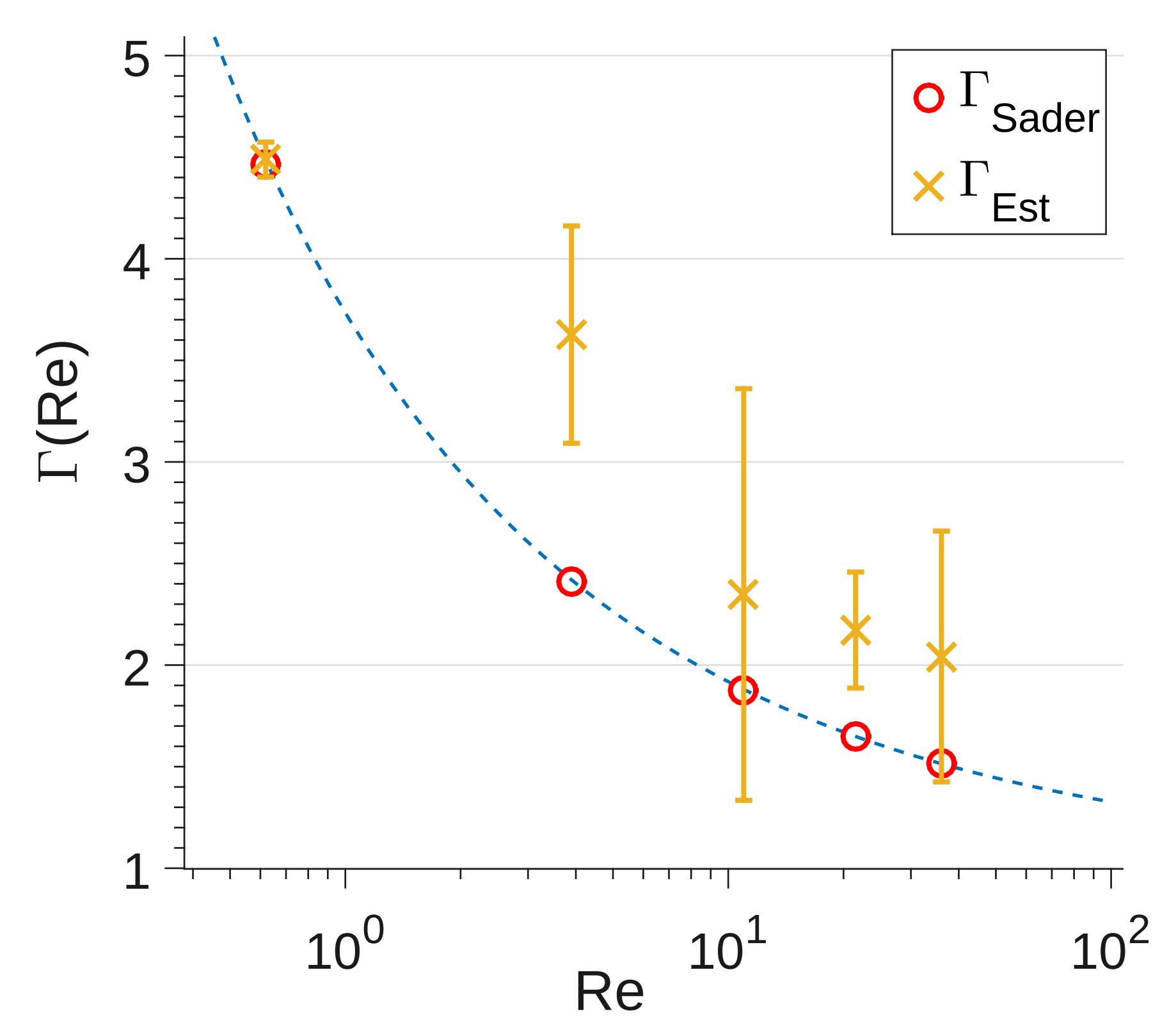
5
4
3
2
1
Γ(Re)
10^0
10^1
10^2
Re
Γ_{Sader}
Γ_{Est}